

1 **Simulation of soil water flow and heat transport in drip irrigated potato field with raised**
2 **beds and full plastic-film mulch in a semiarid area**

3 You-Liang Zhang^{a,b}, Shao-Yuan Feng^{a,b}, Feng-Xin Wang^{b,*}, Andrew Binley^c

4 ^a College of Hydraulic Energy and Power Engineering, Yangzhou University, Yangzhou 225009,
5 China

6 ^b Center for Agricultural Water Research in China, China Agricultural University, No. 17 Qinghua
7 East Road, Haidian, Beijing 100083, China

8 ^c Lancaster Environment Centre, Lancaster University, Lancaster LA1 4YQ, United Kingdom

9 * Corresponding author. Tel.: +86 010 62738523

10 E-mail address: fxinwang@cau.edu.cn (F.-X. Wang)

11 **Abstract**

12 Surface drip irrigation with full plastic-film mulch can increase crop yield and save water by
13 regulating soil water and heat conditions for potato (*Solanum tuberosum* L.) production with
14 raised beds in semiarid area where the rainfall is scarce and evaporation is high. For efficient use
15 of plastic film mulch an understanding of the soil water flow and heat transport is needed. Here we
16 use a model (HYRUS-2D) which is calibrated with field experiments to simulate soil water
17 movement and heat transport. The field experiments were conducted with three treatments,
18 characterized as wetted soil percentages: 35% (P1), 55% (P2), and 75% (P3). Furthermore, the
19 effects of the uncertainty of key soil hydraulic parameters on soil water contents were evaluated
20 using three approaches: (1) soil hydraulic parameters estimated from measured soil textural
21 information (S1); (2) from experimentally measured soil water retention curve (S2); and (3) from
22 inverse modeling (S3). The performance of S2 was the worst in all treatments; the root mean

23 square error (RMSE) was $> 0.05 \text{ cm}^3 \text{ cm}^{-3}$. The performance of S3 was the best with RMSE
24 ranged from 0.015 to $0.038 \text{ cm}^3 \text{ cm}^{-3}$ at 10-50 cm soil depth. The simulated soil water in the raised
25 bed decreased quickly after irrigation, maintaining adequate aeration for potato growth,
26 irrespective of the wetted soil percentage. The downward transport of soil water still existed
27 during the second and third days after irrigation in the simulations of the P2 and P3 treatments.
28 The soil temperatures between the P1 and P3 treatments were similar. In conclusion, the
29 HYDRUS-2D simulations could be used to estimate the soil hydraulic and thermal parameters
30 with inverse modeling. The calibrated model can be used in the design and management of surface
31 drip irrigation with raised beds and full plastic-film mulch to provide favorable soil water and heat
32 conditions for potato growth.

33 **Keywords:** Soil water and heat; Full plastic-film mulch; Surface drip irrigation; Potato; Soil
34 hydraulic parameters; HYDRUS-2D.

35 **1. Introduction**

36 Surface drip irrigation with plastic-film mulching is widely used in agriculture and horticulture.
37 The combination of surface drip irrigation and plastic-film mulching increases water and fertilizer
38 use efficiency and crop yield (Assouline, 2002; Darwish et al., 2003; Tiwari et al., 2003; Phogat et
39 al., 2014). Moreover, plastic-film mulch can modify the radiative and thermal conditions in the
40 fields, which improves plant growth (Liakatas et al., 1986; Wang et al., 2011; Yaghi et al., 2013) .

41 The advantages of this technology depend upon design and management which based on
42 thorough understanding of spatiotemporal distribution of soil water and heat. The main goal is to
43 match the soil wetted volume with root pattern and match soil water storage with crop
44 evapotranspiration (Patel and Rajput, 2008). Many factors can affect the soil wetted volume, such

45 as the soil hydraulic properties, emitter discharge, emitter spacing, wetted soil percentage, etc. The
46 wetted soil percentage is an important parameter used in the design and management of drip
47 irrigation system (Keller and Karmeli, 1974; Zur, 1996). Both soil water and heat stress can affect
48 potato tuber growth, yield, and potato quality (Van Dam et al., 1996; Shock et al., 2007). It is,
49 therefore, important to obtain soil water and heat dynamics in drip irrigated potato field under
50 different wetted soil percentages with raised beds and plastic-film mulch.

51 Field experiments are costly, time-consuming, and site specific (Subbaiah, 2013). Therefore,
52 analytical and numerical modeling methods are widely used to predict the soil water flow and heat
53 transport and spatial-temporal distribution under various conditions (Coelho and Or, 1997; Cook
54 et al., 2003; Šimůnek et al., 2008). Among these models, the HYDRUS model is popular and
55 useful in simulation of soil water flow, solute, and heat transport (Šimůnek et al., 2008). This
56 model has been used to simulate effects of different soil types and fertigation strategies (Gärdenäs
57 et al., 2005; Hanson et al., 2006), emitter discharges (Ajdary et al., 2007), pulsed and continuous
58 irrigation (Phogat et al., 2012; Phogat et al., 2014), bed geometries (Holt et al., 2017), and partial
59 plastic-film mulch (Liu et al., 2013; Chen et al., 2014; Wang et al., 2014; Li et al., 2015a; Li et al.,
60 2015b; Holt et al., 2017; Qi et al., 2018) on soil water and solute transport under surface drip
61 irrigation. The process of soil water and heat transport has also been simulated in winter wheat
62 field with plastic-film mulch under no irrigation (Zhao et al., 2018). However, the effects of
63 different wetted soil percentages on soil water flow and heat transport have not been evaluated
64 with HYDRUS under surface drip irrigation with raised beds and full plastic-film mulch for potato
65 crops. For potatoes in semiarid area, the raised beds and full plastic-film mulching can retain more
66 soil water in plant root zone (Qi et al., 2018) and produce higher yield and water use efficiency in

67 comparison to partial plastic-film mulch (Zhao et al., 2014).

68 Soil hydraulic parameters greatly affect the simulation results of soil water transport. Inverse
69 models can be used to estimate soil hydraulic and thermal parameters (Šimůnek and Genuchten,
70 1996; Hopmans et al., 2002; Mortensen et al., 2006; Nakhaei and Šimůnek, 2014). In this study
71 we validate the applicability of the inverse model with data from potato field. The objectives of
72 this study are to: (1) evaluate the applicability of HDRUS-2D for soil water and heat simulation
73 under drip irrigation with raised beds and full plastic-film mulch; (2) compare simulations of
74 HYDRUS-2D results with soil hydraulic parameters derived from three different approaches
75 (estimated from soil textural information, from experimentally soil water retention curve, and
76 from inverse modeling); and (3) analyze the effects of different wetted soil percentages on soil
77 water and heat transport and spatial-temporal distributions under surface drip irrigation with raised
78 beds and full plastic-film mulch.

79 **2. Materials and methods**

80 2.1. Field experimental site and design

81 Field experiments were carried out at the Shiyanghe Experimental Station of China
82 Agricultural University, located in Wuwei, Gansu Province (N 37°52', E 102°50', altitude 1581 m)
83 from April to August in 2015. This region was characterized by a typical continental temperate
84 climate with mean annual sunshine duration of 3000 hours, mean annual temperature 8 °C, and
85 mean annual accumulated temperature (>0 °C) 3550 °C which was suitable for potato growth.
86 However, agricultural in this region was influenced by scarce water resources with mean annual
87 precipitation of 164 mm, mean annual pan evaporation 2000 mm, and mean groundwater table
88 25-30 m below land surface.

89 Potato plants were drip irrigated in raised beds mulched by transparent plastic film and three
90 wetted soil percentages were designed: 35% (P1), 55% (P2), and 75% (P3). Each treatment was
91 replicated three times.

92 2.2. Agronomic and irrigation practices

93 The specific descriptions of agronomic and irrigation practices have been presented previously
94 (Zhang et al., 2017a; Zhang et al., 2017b). In this manuscript, only main information was included
95 to avoid overlapping. Seed potatoes (30 g, cv. Kexin No.1, Inner Mongolia Minfeng Potato
96 Industry Co., Ltd., Ulanqab, China) were planted every 30 cm in the center of the raised beds at a
97 depth of 15 cm on 15 April 2015. Each plot (6 m × 5.6 m) had 7 north-south raised beds (0.8 m
98 wide and 0.2 m high) which were covered entirely using plastic film mulch (0.008 mm thick, 1.2
99 m wide). In 2015, 231 kg•ha⁻¹ P₂O₅ and 90 kg•ha⁻¹ N were spread before planting and 95 kg•ha⁻¹
100 N and 117 kg•ha⁻¹ K₂O were applied through irrigation after planting.

101 A drip tape (wall thickness 0.4 mm, inner diameter 16 mm) was placed on the soil surface in
102 the center of each bed. The emitter discharge was 1.38 L h⁻¹ at an operating pressure of 0.1 MPa.
103 The drip irrigation system at each plot was managed by a sluice valve, a pressure gauge, a water
104 meter, and a tensiometer. The irrigation application was started when the soil matric potential
105 reached -25 kPa (Wang et al., 2007). The irrigation amount (in mm) was determined using the
106 equation:

$$107 \quad m = h(\theta_a - \theta_b)P / \eta \quad (1)$$

108 where h is the planned wetted depth (cm) (equal to 50 cm for potato plants), θ_a is the volumetric
109 soil water content after irrigation (cm³ cm⁻³) (equal to field capacity 0.27 cm³ cm⁻³ in this
110 experiment), θ_b is the volumetric water content before irrigation (cm³ cm⁻³) (equal to 70% of field

111 capacity), P is the percentage of wetted zone, and η is the coefficient of the efficiency of the drip
112 irrigation system (equal to 0.97 for drip irrigation). The first irrigation amount was 19 mm for all
113 treatments for potato emergence and the subsequent irrigation amount was 15 mm for the P1
114 treatment, 23 mm for the P2 treatment, and 31 mm for the P3 treatment. The actual irrigation
115 amount used for the P1, P2, and P3 treatments was shown in Fig.1.

116 2.3. Weather, soil temperature, and soil water content measurements

117 Meteorological data (precipitation, solar radiation, relative humidity, wind speed, and air
118 temperature) were measured with a standard automatic weather station (HOBO H21-001, Onset
119 Computer Corp., Cape Cod, MA, USA) which was 2 m above the surface of the ground. Before
120 the potato tubers were planted, sensors were installed to measure soil temperature and soil water
121 content. The soil temperatures were measured on the soil surface, and at 5, 10, 20, 30, and 50 cm
122 soil depths both in the middle and at the side (20 cm from the center) of the beds in one replication
123 of each treatment. Soil water contents were measured with sensors at 10, 20, 30, and 50 cm soil
124 depths in the middle, at the side, and at the base (40 cm from the center) of the beds in one
125 replication of each treatment. Sensors on the soil surface and at 5 cm soil depth were
126 thermocouples temperature sensors (ST10, Beijing Unism Technologies, Inc., Beijing, China).
127 Sensors at 10, 20, 30, and 50 cm soil depths in the middle and the side of the beds were soil
128 temperature/water sensors (FDS120, Beijing Unism Technologies, Inc.). Sensors at 10, 20, 30, and
129 50 cm soil depths in the base of the beds were soil water sensors (FDS100, Beijing Unism
130 Technologies, Inc.). The placement of soil water sensors, temperature sensors, and soil
131 temperature/water sensors was shown in Fig.2. The 10 min average soil temperature and soil water
132 content were recorded automatically with a datalogger (SMC6108, Beijing Unism Technologies,

133 Inc.).

134 2.4. Hydraulic parameter measurements

135 Before potato planting, soil samples were taken for soil particle size analysis using a soil auger
136 in the middle of the beds, down to 10, 20, 30, 50, and 70 cm soil depths in each plot. The soil
137 samples were dried in air and sieved with a 2 mm mesh size. Then, soil particle size was analyzed
138 using a Malvern Mastersizer 2000 laser analyzer (Malvern Instruments Ltd., Malvern, UK) (Ryżak
139 and Bieganowski, 2011). Saturated soil water content (θ_s) and bulk density were measured
140 gravimetrically at 0-20 and 20-40 cm soil depths using a ring sampler (diameter 5 cm, height 5.1
141 cm, volume 100 cm³).

142 After potato harvest, three trenches were dug to take soil samples for soil water retention curve
143 (SWRC) measurements. The undisturbed soil samples (diameter 5 cm, height 5.1 cm, volume 100
144 cm³) were taken at 20-40, 40-60, and 60-80 cm soil depths in each trench with three replicates at
145 each layer. Since the shallow soil in the raised beds was disturbed during potato harvest, no soil
146 sample was taken at 0-20 cm soil depth. The soil water retention curve was measured by
147 centrifugation method which has been used widely because of its higher efficiency compared to
148 the ceramic pressure plate method (Šimůnek and Nimmo, 2005; Reatto et al., 2008; Van den Berg
149 et al., 2009; Cropper et al., 2011). The saturated soil samples were centrifuged in a high-speed
150 refrigerated centrifuge (himac CR22G II, Hitachi Koki Co., Ltd., Tokyo, Japan) at different
151 constant rotation speeds (970, 1670, 2160, 2730, 3050, 5290, 6820, 8630, 8830, and 10800 r/min)
152 in sequences for 60 minutes (90 minutes at 8830 and 10800 r/min) to reach the soil water potential
153 equilibrium. The rotation speeds correspond to different matric potentials (-10, -30, -50, -80, -100,
154 -300, -500, -800, -1000, and -1500 kPa). After each centrifugation, the soil samples were weighed

155 and returned to the centrifuge for another higher rotation speed. When the last centrifugation was
156 finished, soil samples were oven-dried at 105 °C to constant dry weight.

157 2.5. Model settings

158 HYDRUS (2D/3D) version 2.05.0200 was applied to simulate soil water and heat transport in
159 the experiments. This code, based on a Galerkin-type linear finite element method, solves
160 Richards' equation for variably-saturated water flow and the advection-dispersion equation for
161 heat and solute transport. The solution also incorporates a sink term in the flow equation to
162 represent root water uptake (Šimůnek et al., 2008; Šimůnek et al., 2016).

163 2.5.1. Numerical modeling theory for soil water flow

164 Since the drip emitter distance was small, the soil water flow can be considered as a
165 two-dimensional problem. Without considering the effect of air phase on liquid flow, the flow is
166 governed by the modified Richards' equation:

$$167 \frac{\partial \theta(h)}{\partial t} = \frac{\partial}{\partial x_i} \left[K(h) \frac{\partial h}{\partial x_j} + K(h) \right] - S(h) \quad (2)$$

168 where θ is the volumetric water content ($\text{cm}^3 \text{ cm}^{-3}$), h is the pressure head (cm), $K(h)$ is the
169 unsaturated hydraulic conductivity function (cm day^{-1}), x_i and x_j are the spatial coordinates x or z
170 (cm), t is time (day) and $S(h)$ is a sink term denoting root water uptake (day^{-1}). The sink term $S(h)$
171 is defined according to the model of Feddes et al. (1978). The unsaturated hydraulic conductivity
172 function is given by the van Genuchten-Mualem model (Mualem, 1976; van Genuchten, 1980).

173 Since the root distribution under drip irrigation is non-uniform, to reflect the spatial variations
174 of root water uptake Vrugt et al. (2001ab) introduced a two-dimensional dimensionless
175 distribution of root water uptake:

$$176 \quad \omega(x, z) = \left(1 - \frac{z}{z_m}\right) \left(1 - \frac{x}{x_m}\right) e^{-\left(\frac{p_z}{z_m} |z^* - z| + \frac{p_x}{x_m} |x^* - x|\right)} \quad (3)$$

177 where z_m denotes the maximum root depth which is set as 50 cm, x_m denotes the maximum root
 178 width which is set as 30 cm, z^* denotes the depth of maximum root intensity which is set as 20 cm,
 179 x^* denotes the width of maximum root intensity which is set as 20 cm, and p_z and p_x are empirical
 180 parameters which is set as 1.

181 2.5.2. Numerical modeling theory for heat transport

182 The two-dimensional heat transport function, ignoring the effects of water vapor, is given by
 183 Sophocleous (1979):

$$184 \quad C(\theta) \frac{\partial T}{\partial t} = \frac{\partial}{\partial x_i} \left[\lambda_{ij}(\theta) \frac{\partial T}{\partial x_j} \right] - C_w q_i \frac{\partial T}{\partial x_i} \quad (4)$$

185 where $\lambda_{ij}(\theta)$ is the soil apparent thermal conductivity ($\text{W cm}^{-1} \text{ } ^\circ\text{C}^{-1}$), $C(\theta)$ is the total volumetric
 186 heat capacity ($\text{J cm}^{-3} \text{ } ^\circ\text{C}^{-1}$), C_w is the volumetric heat capacity of water ($\text{J cm}^{-3} \text{ } ^\circ\text{C}^{-1}$), T is
 187 temperature ($^\circ\text{C}$), and q_i is water flux (cm day^{-1}). In addition, the first and second terms on the
 188 right side of equation (4) represent heat flow due to conduction and heat transported by flowing
 189 water, respectively.

190 The volumetric heat capacity suggested by de Vries (1963) is as follows:

$$191 \quad C(\theta) = C_n \theta_n + C_o \theta_o + C_w \theta + C_g a_v \approx (1.92\theta_n + 2.51\theta_o + 4.18\theta)10^6 \quad (5)$$

192 where the subscripts g , w , o , and n , denote gas phase, liquid phase, organic matter, and solid phase,
 193 respectively.

194 The apparent thermal conductivity $\lambda_{ij}(\theta)$ is described by Šimůnek and Suarez (1993):

$$195 \quad \lambda_{ij}(\theta) = \lambda_T C_w |q| \delta_{ij} + (\lambda_L - \lambda_T) C_w \frac{q_j q_i}{|q|} + \lambda_o(\theta) \delta_{ij} \quad (6)$$

196 where λ_L denotes the longitudinal thermal dispersivity (cm), λ_T denotes the transverse thermal

197 dispersivity (cm), δ_{ij} is the Kronecker delta function, and $\lambda_o(\theta)$ denotes the thermal conductivity.

198 According to Chung and Horton (1987), the $\lambda_o(\theta)$ can be described as follow:

$$199 \quad \lambda_o(\theta) = b_1 + b_2\theta + b_3\theta^{0.5} \quad (7)$$

200 where b_1 , b_2 , and b_3 are empirical parameters ($\text{W cm}^{-1} \text{ }^\circ\text{C}^{-1}$).

201 2.5.3. Soil hydraulic functions and thermal parameters

202 The soil was divided into two layers (0-20 and 20-70 cm soil depths). Three approaches were
203 used to derive the soil hydraulic parameters. Firstly, the Rosetta code (Schaap et al., 2001) in the
204 HYDRUS package was used to estimate the soil hydraulic parameters according to the soil
205 textural distribution and bulk density (Table 1). Secondly, the soil hydraulic parameters at 20-70
206 cm were estimated from the experimentally measured soil water retention curve (Fig.3) fitted by
207 RETC (van Genuchten et al., 1991), while the parameters at 0-20 cm were the same with the first
208 approach. Thirdly, the soil hydraulic parameters were derived with inverse estimation using a
209 Marquardt-Levenberg-type parameter optimization algorithm in HYDRUS-2D. The observed soil
210 water content in the P2 treatment at different soil depths (perpendicular to the drip line at 0, 20 and
211 40 cm and at increments down to 10, 20, 30, 50 cm) during the whole growing season was used to
212 optimize the soil hydraulic parameters (θ_r , α , n , and K_s). The observed θ_s was used and l was set as
213 0.5. The soil water retention curves and soil hydraulic parameters obtained with different
214 approaches were shown in Fig.3 and Table 2, respectively.

215 The thermal parameters b_1 , b_2 , and b_3 were optimized after the soil hydraulic parameters
216 optimization using the observed soil temperature in the P2 treatment at different soil depths
217 (perpendicular to the drip line at 0 and 20 cm and at increments down to 5, 10, 20, 30, 50 cm)
218 during the whole growing season. The thermal parameters were shown in Table 3.

219 2.5.4. Initial and boundary conditions

220 The wetted region on the vertical plane was assumed to be symmetrical on the left and right
221 sides (Chen et al., 2014) and half of the bed was simulated with the drip emitter being placed at
222 the origin of the coordinates (Fig.4). The initial conditions were the volumetric soil water content
223 and temperature measured at different soil depths on 27 May (DAP 42, one day after irrigation).

224 A time variable flux was set on one part of the top soil profile (Or') because of the irrigation.
225 Zero flux was imposed on the other part of the soil surface (r'FED) for water flow because of the
226 plastic-film mulch (Fig.4). Or' is the soil wetted area during irrigation which was computed by an
227 iterative method (Gärdenäs et al., 2005). It was realized by switching from a Neumann to a
228 Dirichlet boundary condition if the pressure head is larger than zero as the emitter flux was applied
229 (Gärdenäs et al., 2005). Different soil wetted lengths can be obtained for different irrigation fluxes
230 and initial soil water contents. After irrigation, the whole soil surface of the upper boundary
231 condition was imposed as zero flux because of the plastic-film mulch. A free drainage boundary
232 condition was used for the lower boundary condition because of assumed deep ground water.
233 No-flow boundary conditions were prescribed on the left and right sides, assuming that no flow
234 took place along the perpendicular sides. The third type, Cauchy, and the first type, Dirichlet,
235 boundary conditions were used on Or' and the other part of the top soil profile (r'FED) for heat
236 transport, respectively. No flux boundary conditions were assumed on both sides and third type
237 boundary on the bottom of the profile for heat transport.

238 2.5.5. Evapotranspiration

239 The daily crop evapotranspiration (ET_c) was calculated using the dual crop coefficient method
240 and Penman-Monteith equation (Allen et al., 1998):

241 $ET_c = (K_{cb} + K_e)ET_o$ (8)

242 where ET_o is reference crop evapotranspiration calculated according to the meteorological data,
 243 K_{cb} is the basal crop coefficient for crop transpiration, and K_e is the coefficient for soil evaporation.
 244 The basal crop coefficient (K_{cb}) used for each growth stage was based on the recommended value
 245 by FAO and the actual crop growth. In addition, K_{cb} was 10% larger for crop grown with plastic
 246 film mulch than without plastic film mulch according to the guidelines (Allen et al., 1998). The
 247 daily transpiration (Fig.1) was used as a time-variable boundary condition. Soil evaporation was
 248 neglected because of the full plastic-film mulch.

249 2.5.6. Model performance

250 The model efficiency was evaluated by the root mean square errors ($RMSE$), the mean absolute
 251 errors (MAE), and the mean relative errors (MRE):

252 $RMSE = \sqrt{\frac{1}{N} \sum_{i=1}^N (P_i - O_i)^2}$ (9)

253

254 $MAE = \frac{1}{N} \sum_{i=1}^N |P_i - O_i|$ (10)

255

256 $MRE = \frac{1}{N} \sum_{i=1}^N \left| \frac{P_i - O_i}{O_i} \right|$ (11)

257 where N is the number of observations, P_i is the simulated value, and O_i is the observed value.

258 **3. Results and discussion**

259 3.1. Calibration and validation

260 3.1.1. Soil water content simulation

261 The model parameters were calibrated with data of the P2 treatment and the model was

262 validated with data of the P1 and P3 treatments. Soil water contents were simulated with soil
263 hydraulic parameters estimated from soil textural information (S1). According to Phogat et al.
264 (2012) the RMSE used to evaluate the satisfaction of soil water content simulation is 0.05 cm^3
265 cm^{-3} . The performance of S1 for the P1 treatment was not satisfactory because the RMSE of S1 at
266 five positions were larger than $0.05 \text{ cm}^3 \text{ cm}^{-3}$. The simulated soil water contents of S1 agreed
267 reasonably well with the observed data for the P2 treatment. The RMSE of S1 ranged from 0.014
268 to $0.039 \text{ cm}^3 \text{ cm}^{-3}$ with the MRE from 7.1% to 19.9% for the P2 treatment (Table 4). For the P3
269 treatment the performance of S1 was good for most of the positions with the RMSE ranged from
270 0.016 to $0.048 \text{ cm}^3 \text{ cm}^{-3}$ except two positions (10 cm soil depth on the top of the bed and 50 cm
271 soil depth on the base of the bed with the $\text{RMSE} > 0.05 \text{ cm}^3 \text{ cm}^{-3}$). The simulated soil water
272 contents of S1 were overestimated at 0-10 cm soil depth on the top and the side of the bed and
273 underestimated at 50 cm soil depth in the base of the bed for the P3 treatment (Fig.5).

274 Soil water contents were simulated using parameters estimated from measured soil water
275 retention curve (S2). The performance of S2 was not satisfactory for the three treatments because
276 the RMSE at nine positions for the P1 treatment, four positions for the P2 treatment, and ten
277 positions for the P3 treatment were $> 0.05 \text{ cm}^3 \text{ cm}^{-3}$ (Table 4). Dahiya et al. (2007) also reported
278 that the simulation results with experimentally measured soil water retention curve and hydraulic
279 conductivity were not satisfactory.

280 Soil water contents were simulated with parameters derived from inverse model (S3). The
281 performance of S3 was not satisfactory for the P1 treatment with the RMSE at five positions larger
282 than $0.05 \text{ cm}^3 \text{ cm}^{-3}$. The RMSE of S3 for the P2 treatment ranged from 0.017 to $0.049 \text{ cm}^3 \text{ cm}^{-3}$
283 with the MRE from 6.9% to 20.1%. The simulated soil water contents of S3 at 50 cm soil depth in

284 the base of the bed were underestimated for the P3 treatment and the RMSE was quite large (0.078
285 $\text{cm}^3 \text{cm}^{-3}$). The RMSE of S3 at the other soil depths ranged from 0.015 to 0.038 $\text{cm}^3 \text{cm}^{-3}$ for the
286 P3 treatment with the MRE from 6.9% to 20.8%.

287 Both the S1 and S3 did not have good simulation results for the P1 treatment and at 50 cm soil
288 depth in the base of the bed of the P3 treatment. This might be because the soil properties in these
289 positions were much different to those of the overall soil. The reason for the unsatisfactory
290 simulation of S2 might be caused by the scale effects of the ring sample size (Zhao et al., 2010).
291 Comparing with S3, the performance of S1 was poor at 10 cm soil depth. This might be because
292 the hydraulic conductivity estimated from the soil textural information was smaller than the actual
293 value. Overall, as the inverse model could adjust the soil hydraulic parameters effectively to fit the
294 observed soil water contents, the performance of S3 was the best.

295 3.1.2. Soil heat simulation

296 Generally, the simulation of soil temperatures with thermal parameters estimated by heat
297 transport inverse model was reasonably good (Table 5 and Fig.6). The RMSE of soil temperature
298 at 5 cm soil depth (ranged from 2.0 to 4.2 $^{\circ}\text{C}$) was large. The large errors might be caused by the
299 insufficient contact of the soil temperature sensors at 5 cm soil depth. The RMSE of soil
300 temperatures at 10-50 cm soil depth ranged from 1.0 to 2.5 $^{\circ}\text{C}$ with the MRE from 4.4% to 13%
301 for the P1 treatment; the RMSE ranged from 1.1 to 2.5 $^{\circ}\text{C}$ with the MRE from 5.5% to 10.6%
302 (except at 20 cm soil depth) for the P2 treatment; and the RMSE from 1.2 to 2.2 $^{\circ}\text{C}$ with the MRE
303 from 4.5% to 12.7% for the P3 treatment. Unlike the simulations of soil water, the simulations of
304 soil temperatures in all treatments were satisfactory. This result indicated that the spatial
305 heterogeneity in thermal parameters in the field was less than in soil hydraulic parameters. It was

306 consistent with the report of Dahiya et al. (2007).

307 3.2. Soil water transport and distribution

308 Soil water distributions at the end of irrigation and during the following three days after the
309 irrigation were simulated with the soil hydraulic parameters estimated by inverse modeling (Fig.7).
310 The higher wetted soil percentage of drip irrigation led to a larger soil wetted zone. At the end of
311 irrigation the depth of soil wetted front (soil water content equal to $0.22 \text{ cm}^3 \text{ cm}^{-3}$) was 24 cm for
312 the P1 treatment, 27 cm for the P2 treatment, and 31 cm for the P3 treatment. The horizontal
313 distance of the soil wetted front at 20 cm depth was 12 cm for the P1 treatment, 17 cm for the P2
314 treatment, and 23 cm for the P3 treatment. The larger difference of the soil wetted front in the
315 horizontal direction meant that the high wetted soil percentage accelerated the horizontal soil
316 water transport more than the vertical soil water transport.

317 After irrigation, the soil water content reduced rapidly at 0-20 cm soil depth during the first
318 day because of the larger soil hydraulic conductivity at the raised bed. The smaller soil water
319 content meant adequate aeration for potato tubers. It was one of the reasons why the raised bed
320 could benefit potato growth (Harms and Korschuh, 2010). During the second and third days after
321 irrigation, there was soil water downward transport for the P2 and P3 treatments but not for the P1
322 treatment. This meant that a higher wetted soil percentage could cause more deep percolation. The
323 wetted soil percentage of 35% (P1) was enough for the potato growth in this area.

324 3.3. Soil temperature transport and distribution

325 The soil temperatures between the P1 and P3 treatments were similar, although the average
326 soil temperature for the P1 treatment was 0.1-0.7 °C higher than for the P3 treatment (Fig.8). Li et
327 al. (2017) also reported small soil temperature differences in different irrigation treatments. The

328 soil temperature for the P2 treatment was the lowest among the three treatments. This result was
329 reasonable as soil temperature could be affected not only by the soil moisture but also by the plant
330 canopy. The potato plant canopy varied too much in the field: the lowest soil temperature for the
331 P2 treatment might be caused by the larger canopy around the soil temperature sensors.

332 **4. Summary and conclusion**

333 In this study, HYDRUS-2D was used to simulate soil water and heat transport in a potato field
334 under surface drip irrigation with raised beds and full plastic-film mulch. Three approaches were
335 used to evaluate the soil water simulation with parameters derived from soil textural information
336 (S1), from experimentally measured soil water retention curve (S2), and from inverse modeling
337 (S3). All the three approaches performed unsatisfactorily for the P1 treatment and at 50 cm soil
338 depth in the base of the bed for the P3 treatment because of the soil spatial heterogeneity. The
339 performance of S2 was the worst for all treatments, giving a high RMSE ($> 0.05 \text{ cm}^3 \text{ cm}^{-3}$). The
340 performance of S1 was much better than S2 with an RMSE ranged from 0.014 to 0.039 $\text{cm}^3 \text{ cm}^{-3}$
341 at 10-50 cm soil depth for the P2 treatment and from 0.016 to 0.048 $\text{cm}^3 \text{ cm}^{-3}$ at 20-50 cm soil
342 depth (except at 50 cm soil depth in the base of the bed) for the P3 treatment. The performance of
343 S3 was better than S1, especially at 0-10 cm soil depth. The RMSE of S3 for the P3 treatment
344 ranged from 0.015 to 0.038 $\text{cm}^3 \text{ cm}^{-3}$ at 10-50 cm soil depth (except at 50 cm soil depth in the base
345 of the bed). The soil temperature simulation with thermal parameters estimated by inverse model
346 was satisfactory with the RMSE ranged from 1.0 to 2.5 °C at 10-50 cm soil depth (except at 20 cm
347 soil depth for the P2 treatment).

348 The simulated soil water in the raised bed decreased quickly after irrigation, which could
349 maintain adequate aeration for potato growth, irrespective of the wetted soil percentage. The

350 downward transport of soil water still existed on the second and third days after irrigation for the
351 P2 and P3 treatments. The soil temperatures between the P1 and P3 treatments were similar. The
352 large soil temperature difference could be caused by plant canopy differences. Generally, a wetted
353 soil percentage of 35% could provide suitable soil water and heat conditions under surface drip
354 irrigation with raised beds and full plastic-film mulch for potato growth in this area.

355 In conclusion, the HYDRUS-2D could be used to simulate soil water flow and heat transport
356 in drip irrigated potato field with raised beds and full plastic-film mulch. Furthermore, the
357 calibrated HYDRUS-2D was useful to derive the distribution of soil water and heat under different
358 combination of emitter distance and discharge and irrigation scheduling for potato production.

359 **Acknowledgements**

360 The financial support of this study came from Program 201501017 of the Ministry of Water
361 Resources of China and Program 51579240 of National Natural Science Foundation of China. The
362 first author studied the model in Lancaster University from April 2016 to October 2016 supported
363 by China Scholarship Council (CSC), British Council (BC), and Newton Fund.

364 **References**

- 365 Ajdary, K., Singh, D.K., Singh, A.K., Khanna, M., 2007. Modelling of nitrogen leaching from
366 experimental onion field under drip fertigation. *Agric. Water Manage.* 89, 15-28.
- 367 Allen, R.G., Pereira, L.S., Raes, D., Smith, M., 1998. *Crop evapotranspiration: Guidelines for*
368 *computing crop water requirements.* FAO Irrigation and drainage paper No. 56, FAO, Rome, Italy.
- 369 Assouline, S., 2002. The effects of microdrip and conventional drip irrigation on water distribution and
370 uptake. *Soil Sci. Soc. Am. J.* 66, 1630-1636.
- 371 Chen, L.J., Feng, Q., Li, F.R., Li, C.S., 2014. A bidirectional model for simulating soil water flow and

372 salt transport under mulched drip irrigation with saline water. *Agric. Water Manage.* 146, 24-33.

373 Chung, S.O., Horton, R., 1987. Soil heat and water flow with a partial surface mulch. *Water Resour.*
374 *Res.* 23(12), 2175-2186.

375 Coelho, F.E., Or, D., 1997. Applicability of analytical solutions for flow from point sources to drip
376 irrigation management. *Soil Sci. Soc. Am. J.* 61, 1331-1341.

377 Cook, F.J., Thorburn, P.J., Bristow, K.L., Cote, C.M., 2003. Infiltration from surface and buried point
378 sources: the average wetting water content. *Water Resour. Res.* 39, 1364-1369.

379 Cropper, S.C., Perfect, E., van den Berg, E.H., Mayes, M.A., 2011. Comparison of average and point
380 capillary pressure-saturation functions determined by steady-state centrifugation. *Soil Sci. Soc. Am. J.*
381 75(1), 17-25.

382 Dahiya, R., Ingwersen, J., Streck, T., 2007. The effect of mulching and tillage on the water and
383 temperature regimes of a loess soil: Experimental findings and modeling. *Soil Till. Res.* 96, 52-63.

384 Darwish, T., Atallah, T., Hajhasan, M., Chranek, S., 2003. Management of nitrogen by fertigation of
385 potato in Lebanon. *Nutr. Cycl. Agroecosys.* 67, 1-11.

386 de Vries, D.A., 1963. The thermal properties of soils, In *Physics of Plant Environment*, edited by R.W.
387 van Wijk, pp. 210-235, North Holland, Amsterdam.

388 Feddes, R.A., Kowalik, P.J., Zaradny, H., 1978. *Simulation of Field Water Use and Crop Yield*. John
389 Wiley and Sons, New York, NY.

390 Gärdenäs, A.I., Hopmans, J.W., Hanson, B.R., Šimůnek, J., 2005. Two-dimensional modeling of nitrate
391 leaching for various fertigation scenarios under micro-irrigation. *Agric. Water Manage.* 74, 219-242.

392 Hanson, B.R., Šimůnek, J., Hopmans, J.W., 2006. Evaluation of urea - ammonium - nitrate fertigation
393 with drip irrigation using numerical modeling. *Agric. Water Manage.* 86, 102-113.

394 Harms, T.E., Korschuh, M.N., 2010. Water savings in irrigated potato production by varying
395 hill-furrow or bed-furrow configuration. *Agric. Water Manage.* 97, 1399-1404.

396 Holt, N., Shukla, S., Hochmuth, G., Muñoz-Carpena, R., Ozores-Hampton, M., 2017. Transforming the
397 food-water-energy-land-economic nexus of plasticulture production through compact bed geometries.
398 *Adv. Water Resour.* 110, 515-527.

399 Hopmans, J.W., Šimunek, J., Bristow, K.L., 2002. Indirect estimation of soil thermal properties and
400 water flux using heat pulse probe measurements: Geometry and dispersion effects. *Water Resour. Res.*
401 38(1), 7, 1-7, 14.

402 Keller, J., Karmeli, D., 1974. Trickle irrigation design parameters. *T. ASAE* 17, 678-684.

403 Li, X.W., Jin, M.G., Huang, J.O., Yuan, J.J., 2015a. The soil-water flow system beneath a cotton field
404 in arid north-west China, serviced by mulched drip irrigation using brackish water. *Hydrogeol. J.* 23,
405 35-46.

406 Li, X.Y., Shi, H.B., Šimunek, J., Gong, X.W., Peng, Z.Y., 2015b. Modeling soil water dynamics in a
407 drip-irrigated intercropping field under plastic mulch. *Irrig. Sci.* 33(4), 289-302.

408 Li, X.Y., Šimunek, J., Shi, H.B., Yan, J.W., Peng, Z.Y., Gong, X.W., 2017. Spatial distribution of soil
409 water, soil temperature, and plant roots in a drip-irrigated intercropping field with plastic mulch. *Europ.*
410 *J. Agronomy* 83, 47-56.

411 Liakatas, A., Clark, J.A., Monteith, J.L., 1986. Measurements of the heat balance under plastic mulches.
412 Part I. Radiation balance and soil heat flux. *Agric. For. Meteorol.* 36, 223-227.

413 Liu, M.X., Yang, J.S., Li, X.M., Yu, M., Wang, J., 2013. Numerical simulation of soil water dynamics
414 in a drip irrigated cotton field under plastic mulch. *Pedosphere* 23(5), 620-635.

415 Mortensen, A.P., Hopmans, J.W., Mori, Y., Šimunek, J., 2006. Multi-functional heat pulse probe

416 measurements of coupled vadose zone flow and transport. *Adv. Water Resour.* 29, 250-267.

417 Mualem, Y., 1976. A new model for predicting the hydraulic conductivity of unsaturated porous media.

418 *Water Resour. Res.* 12(3), 513-522.

419 Nakhaei, M., Šimůnek, J., 2014. Parameter estimation of soil hydraulic and thermal property functions

420 for unsaturated porous media using the HYDRUS-2D code. *J. Hydrol. Hydromech.* 62(1), 7-15.

421 Patel, N., Rajput, T.B.S., 2008. Dynamics and modeling of soil water under subsurface drip irrigated

422 onion. *Agric. Water Manage.* 95, 1335-1349.

423 Phogat, V., Mahadevan, M., Skewes, M., Cox, J.W., 2012. Modelling soil water and salt dynamics

424 under pulsed and continuous surface drip irrigation of almond and implications of system design. *Irrig.*

425 *Sci.* 30, 315-333.

426 Phogat, V., Skewes, M.A., Cox, J.W., Sanderson, G., Alam, J., Šimůnek, J., 2014. Seasonal simulation

427 of water, salinity and nitrate dynamics under drip irrigated mandarin (*Citrus reticulata*) and assessing

428 management options for drainage and nitrate leaching. *J. Hydrol.* 513, 504-516.

429 Qi, Z.J., Feng, H., Zhao, Y., Zhang, T.B., Yang, A.Z., Zhang, Z.X., 2018. Spatial distribution and

430 simulation of soil moisture and salinity under mulched drip irrigation combined with tillage in an arid

431 saline irrigation district, northwest China. *Agric. Water Manage.* 201, 219-231.

432 Reatto, A., Da Silva, E.M., Bruand, A., Martins, E.S., Lima, J.E.F.W., 2008. Validity of the centrifuge

433 method for determining the water retention properties of tropical soils. *Soil Sci. Soc. Am. J.* 72(6),

434 1547-1553.

435 Ryzak, M., Bieganski, A., 2011. Methodological aspects of determining soil particle-size

436 distribution using the laser diffraction method. *J. Plant Nutr. Soil Sci.* 174, 624-633.

437 Schaap, M.G., Leij, F.J., van Genuchten, M.T., 2001. Rosetta: a computer program for estimating soil

438 hydraulic parameters with hierarchical pedotransfer functions. *J. Hydrol.* 251, 163-176.

439 Shock, C.C., Pereira, A.B., Eldredge, E.P., 2007. Irrigation best management practices for potato. *Am.*
440 *J. Potato Res.* 84, 29-37.

441 Šimůnek, J., Genuchten, M.T., 1996. Estimating unsaturated soil hydraulic properties from tension disc
442 infiltrometer data by numerical inversion. *Water Resour. Res.* 32(9), 2683-2696.

443 Šimůnek, J., Nimmo, J.R., 2005. Estimating soil hydraulic parameters from transient flow experiments
444 in a centrifuge using parameter optimization technique. *Water Resour. Res.* 41, W04015.

445 Šimůnek, J., Suarez, D.L., 1993. UNSATCHEM-2D code for simulating two-dimensional variably
446 saturated water flow, heat transport, carbon dioxide production and transport, and multicomponent
447 solute transport with major ion equilibrium and kinetic chemistry, Version 1.1, Research Report No.
448 128, U. S. Salinity Laboratory, USDA, ARS, Riverside, CA.

449 Šimůnek, J., van Genuchten, M.T., Šejna, M., 2008. Development and applications of the HYDRUS
450 and STANMOD software packages and related codes. *Vadose Zone J.* 7(2), 587-600.

451 Šimůnek, J., van Genuchten, M. T., Šejna, M., 2016. Recent developments and applications of the
452 HYDRUS computer software packages. *Vadose Zone J.* 15(7), pp.25.

453 Sophocleous, M., 1979. Analysis of water and heat flow in unsaturated-saturated porous media. *Water*
454 *Resour. Res.* 15(5), 1195-1206.

455 Subbaiah, R., 2013. A review of models for predicting soil water dynamics during trickle irrigation.
456 *Irrig. Sci.* 31, 225-258.

457 Tiwari, K.N., Singh, A., Mal, P.K., 2003. Effect of drip irrigation on yield of cabbage (*Brassica*
458 *oleracea* L. var. *capitata*) under mulch and non-mulch conditions. *Agric. Water Manage.* 58, 19-28.

459 Van Dam, J., Kooman, P.L., Struik, P.C., 1996. Effects of temperature and photoperiod on early

460 growth and final number of tubers in potato (*Solanum tuberosum* L.). Potato Res. 39, 51-62.

461 Van den Berg, E.H., Perfect, E., Tu, C., Knappett, P.S.K., Leao, T.P., Donat, R.W., 2009. Unsaturated
462 hydraulic conductivity measurements with centrifuges: a review. Vadose Zone J. 8(3), 531-547.

463 van Genuchten, M.T., 1980. A closed-form equation for predicting the hydraulic conductivity of
464 unsaturated soils. Soil Sci. Soc. Am. J. 44, 892-898.

465 van Genuchten, M.T., Leij, F.J., Yates, S.R., 1991. The RETC Code for Quantifying the Hydraulic
466 Functions of Unsaturated Soils, Version 1.0. EPA Report 600/2-91/065, U.S. Salinity Laboratory,
467 USDA, ARS, Riverside, California.

468 Vrugt, J.A., Hopmans, J.W., Šimůnek, J., 2001a. Calibration of a two-dimensional root water uptake
469 model. Soil Sci. Soc. Am. J. 65(4), 1027-1037.

470 Vrugt, J.A., van Wijk, M.T., Hopmans, J.W., Šimůnek, J., 2001b. One-, two-, and three-dimensional
471 root water uptake functions for transient modeling. Water Resour. Res. 37(10), 2457-2470.

472 Wang, F.X., Kang, Y.H., Liu, S.P., Hou, X.Y., 2007. Effects of soil matric potential on potato growth
473 under drip irrigation in the North China Plain. Agric. Water Manage. 88, 34-42.

474 Wang, F.X., Wu, X.X., Shock, C.C., Chu, L.Y., Gu, X.X., Xue, X., 2011. Effects of drip irrigation
475 regimes on potato tuber yield and quality under plastic mulch in arid Northwestern China. Field Crops
476 Res. 122, 78-84.

477 Wang, Z.M., Jin, M.G., Šimůnek, J., van Genuchten, M.T., 2014. Evaluation of mulched drip irrigation
478 for cotton in arid Northwest China. Irrig. Sci. 32, 15-27.

479 Yaghi, T., Arslan, A., Naoum, F., 2013. Cucumber (*Cucumis sativus*, L.) water use efficiency (WUE)
480 under plastic mulch and drip irrigation. Agric. Water Manage. 128, 149-157.

481 Zhang, Y.L., Wang, F.X., Shock, C.C., Yang, K.J., Kang, S.Z., Qin, J.T., Li, S.E., 2017a. Effects of

482 plastic mulch on the radiative and thermal conditions and potato growth under drip irrigation in arid
483 Northwest China. *Soil Till. Res.* 172, 1-11.

484 Zhang, Y.L., Wang, F.X., Shock, C.C., Yang, K.J., Kang, S.Z., Qin, J.T., Li, S. E., 2017b. Influence of
485 different plastic film mulches and wetted soil percentages on potato grown under drip irrigation. *Agric.*
486 *Water Manage.* 180, 160-171.

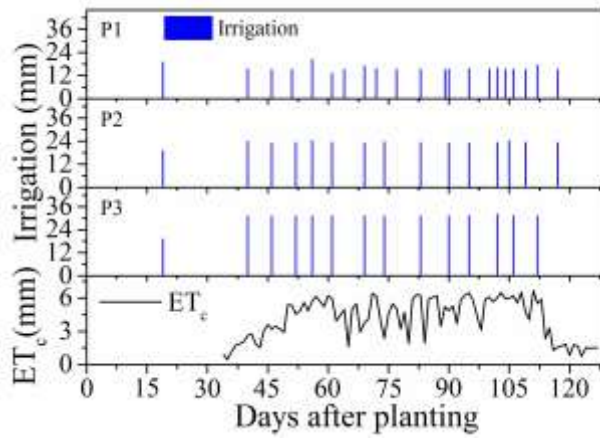
487 Zhao, H., Wang, R.Y., Ma, B.L., Xiong, Y.C., Qiang, S.C., Wang, C.L., A., L.C., Li, F.M., 2014.
488 Ridge-furrow with full plastic film mulching improves water use efficiency and tuber yields of potato
489 in a semiarid rainfed ecosystem. *Field Crops Res.* 161, 137-148.

490 Zhao, Y., Peth, S., Horn, R., Krümmelbein, J., Ketzer, B., Gao, Y.Z., Doerner, J., Bernhofer, C., Peng,
491 X.H., 2010. Modeling grazing effects on coupled water and heat fluxes in Inner Mongolia grassland.
492 *Soil Till. Res.* 109, 75-86.

493 Zhao, Y., Zhai, X.F., Wang, Z.H., Li, H.J., Jiang, R., Hill, R.L., Si, B., Feng, H., 2018. Simulation of
494 soil water and heat flow in ridge cultivation with plastic film mulching system on the Chinese Loess
495 Plateau. *Agric. Water Manage.* 202, 99-112.

496 Zur, B., 1996. Wetted soil volume as a design objective in trickle irrigation. *Irrig. Sci.* 16, 101-105.

497
498
499
500
501
502
503
504
505



506

507 **Fig.1.** The amount of each irrigation in 35% soil wetted treatment (P1), 55% soil wetted treatment
 508 (P2), and 75% soil wetted treatment (P3). The actual daily evapotranspiration (ET_c) during the
 509 growing season.

510

511

512

513

514

515

516

517

518

519

520

521

522

523

524

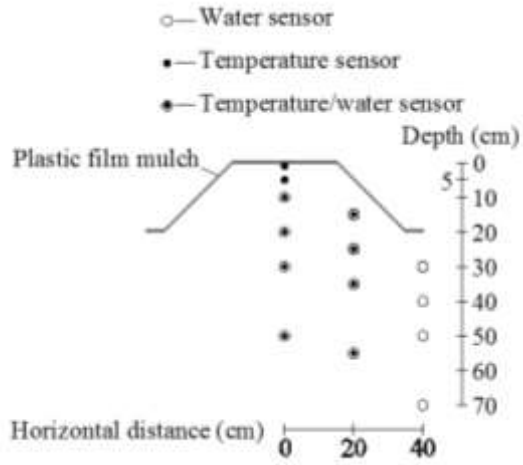
525

526

527

528

529



530

531 **Fig.2.** Placement of soil water sensors, temperature sensors, and soil temperature/water sensors.

532

533

534

535

536

537

538

539

540

541

542

543

544

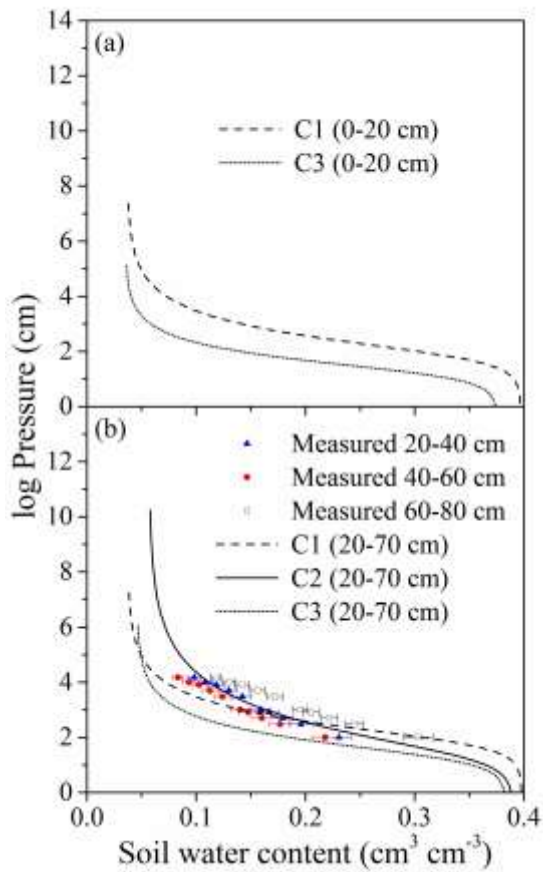
545

546

547

548

549



550

551 **Fig.3.** Soil water retention curves estimated by measured soil textural information (C1), measured
 552 experimentally (C2) (measured at 20-40 cm, 40-60 cm, and 60-80 cm soil depths), and estimated
 553 by inverse modeling (C3) at: (a) 0-20 cm soil depth; and (b) 20-70 cm soil depth.

554 **Note:** Soil water retention curve was not experimentally measured at 0-20 cm soil depth.

555

556

557

558

559

560

561

562

563

564

565

566

567

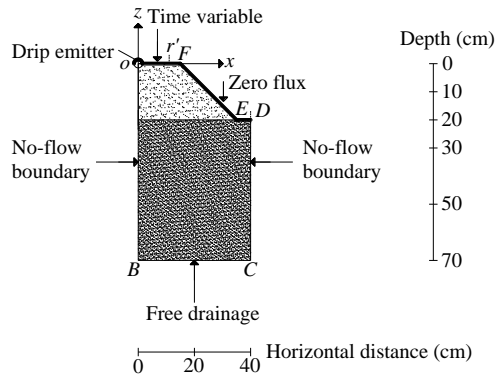
568

569

570

571

572



573

574 **Fig.4.** Scale diagram of the simulated domain and boundary conditions.

575

576

577

578

579

580

581

582

583

584

585

586

587

588

589

590

591

592

593

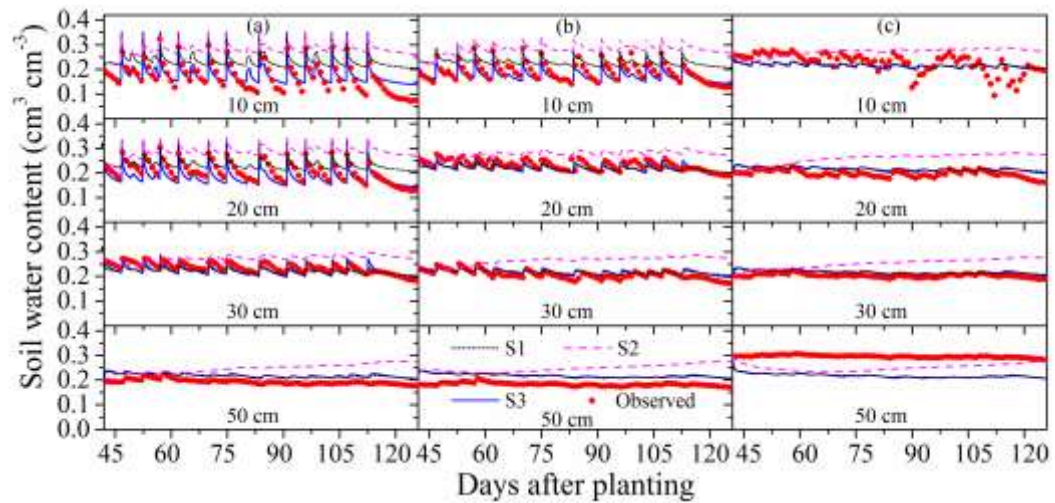
594

595

596

597

598



599

600 **Fig.5.** Observed and simulated daily soil water content at different depths in (a) the top, (b) the
 601 side, and (c) the base of the bed for the P3 treatment with three simulation approaches: simulation
 602 with parameters estimated from soil textural information (S1), from experimentally measured soil
 603 water retention curve (S2), and from inverse modeling (S3).

604

605

606

607

608

609

610

611

612

613

614

615

616

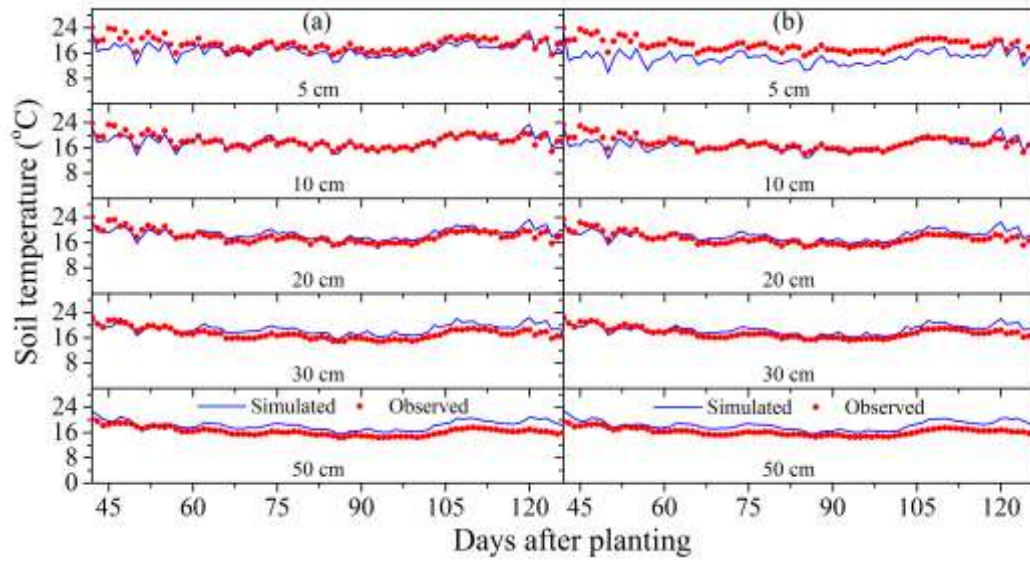
617

618

619

620

621



622

623 **Fig.6.** Observed and simulated daily soil temperatures at different depths in (a) the top and (b) the
 624 side of the bed for the P3 treatment with simulation using parameters estimated from inverse
 625 modeling.

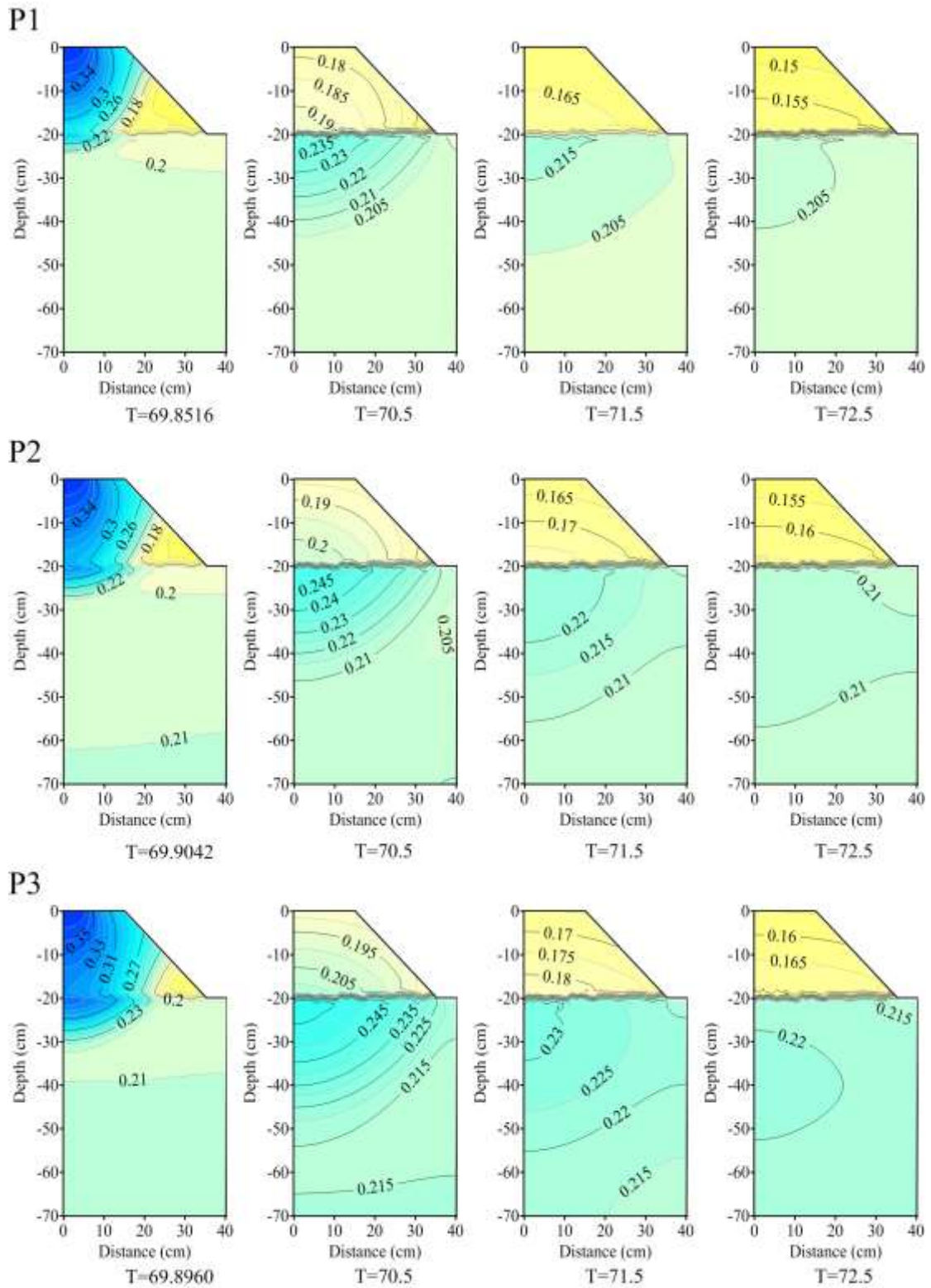
626

627

628

629

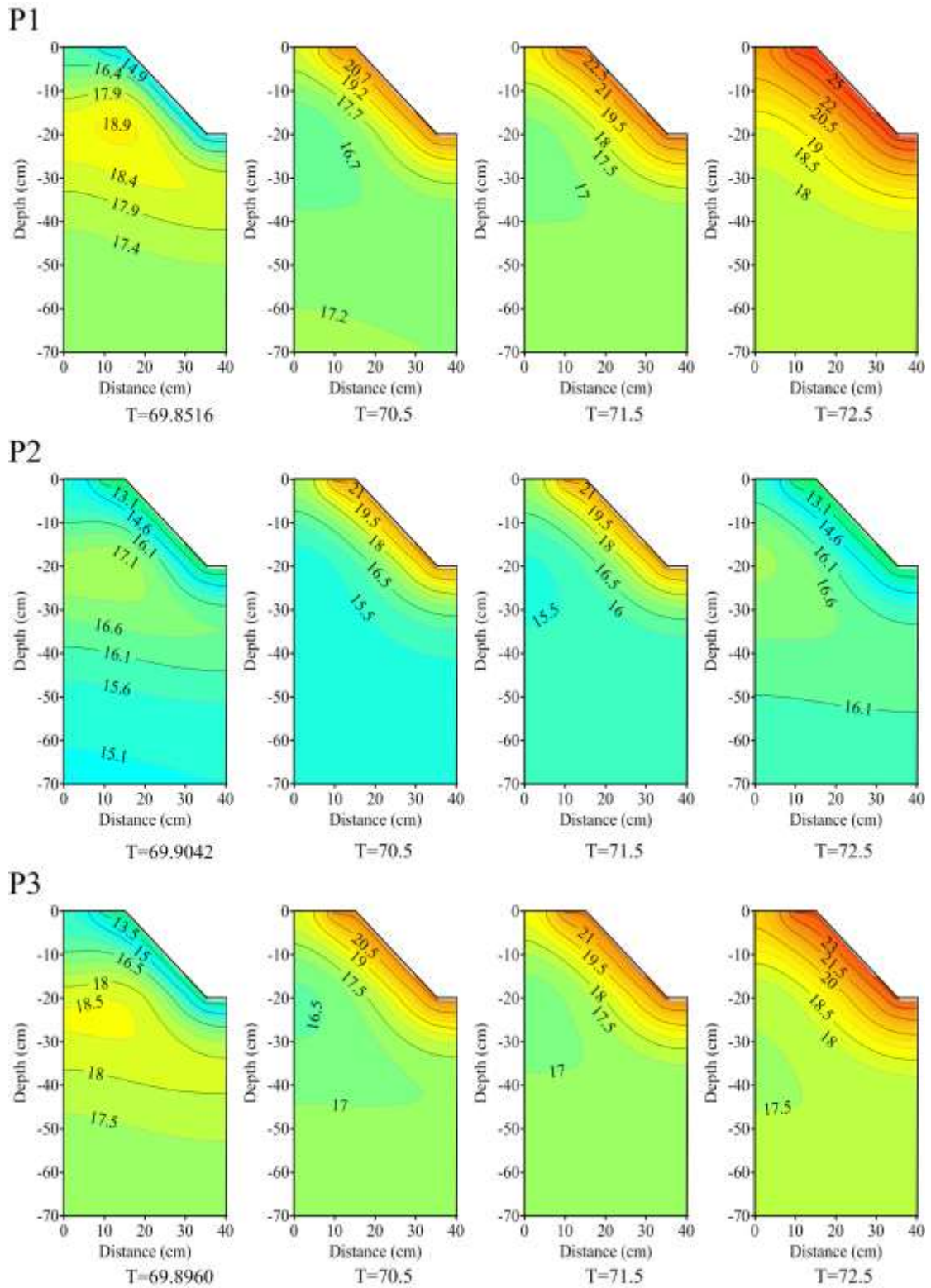
630



631

632 **Fig.7.** Simulated soil water distributions at the end of irrigation (on 69.8516 days after planting for
 633 the P1 treatment, 69.9042 days for the P2 treatment, 69.8960 days for the P3 treatment) and the
 634 following three days after the irrigation (on 70.5 days, 71.5 days, and 72.5 days after planting) for
 635 the P1, P2, and P3 treatments.

636



637

638 **Fig.8.** Simulated soil temperature distributions at the end of irrigation (on 69.8516 days after
 639 planting for the P1 treatment, 69.9042 days for the P2 treatment, 69.8960 days for the P3
 640 treatment) and the following three days after the irrigation (on 70.5 days, 71.5 days, and 72.5 days
 641 after planting) for the P1, P2, and P3 treatments.

642

643

644
645
646
647
648
649
650
651
652
653
654
655
656
657
658
659
660
661
662
663
664
665
666
667
668
669
670
671
672
673
674
675
676
677
678
679

Table 1

Soil grain size distribution, bulk density, and saturated water content (θ_s) at different depths.

Depth (cm)	Sand (%)	Silt (%)	Clay (%)	Soil type	Bulk density (g cm ⁻³)	θ_s (cm ³ cm ⁻³)
	2-0.05 mm	0.05-0.002 mm	< 0.002 mm			
0-10	51.2 (5.4 ^a) NS	41.4 (4.8 ^a) NS	7.4 (0.7 ^a) NS	Loam	1.48 (0.05 ^b)	0.375 (0.009 ^b)
10-20	51.0 (7.9)	41.6 (6.7)	7.4 (1.6)	Loam		
20-30	52.7 (2.7)	39.9 (2.2)	7.4 (0.5)	Sandy Loam	1.58 (0.06)	0.383 (0.033)
30-50	50.0 (4.4)	42.3 (3.7)	7.7 (0.7)	Loam		
50-70	46.9 (5.8)	45.3 (5.1)	7.8 (0.8)	Loam		

NS: difference among different depths was not significant by F-test ($P > 0.05$);

^a Values in parentheses denoted the standard deviation with n = 15;

^b Values in parentheses denoted the standard deviation with n = 9.

680 **Table 2**

681 Soil hydraulic parameters (the residual water content θ_r , the saturated water content θ_s , the
 682 saturated hydraulic conductivity K_s , and empirical coefficients α , n , and l) estimated from
 683 measured soil textural information (S1), from experimentally measured soil water retention curve
 684 (S2), and from inverse modeling (S3).

Depth (cm)	θ_r (cm ³ cm ⁻³)	θ_s (cm ³ cm ⁻³)	α (cm ⁻¹)	n	K_s (cm day ⁻¹)	l
S1						
0-20	0.0371	0.397	0.0137	1.471	35.31	0.5
20-70	0.0377	0.398	0.0127	1.485	34.88	0.5
S2						
0-20	0.0371	0.397	0.0137	1.471	35.31	0.5
20-70	0.0517	0.390	0.0508	1.290	34.88	0.5
S3						
0-20	0.0354	0.375	0.0557	1.672	176.90	0.5
20-70	0.0459	0.383	0.0476	1.549	50.72	0.5

685
 686
 687
 688
 689
 690
 691
 692
 693
 694
 695
 696
 697
 698
 699
 700
 701
 702
 703
 704
 705
 706

707

Table 3

708

Soil thermal parameters (the volumetric solid phase fraction θ_n , the volumetric organic matter

709

fraction θ_o , the longitudinal thermal dispersivity λ_L , the transverse thermal dispersivity λ_T , the

710

volumetric heat capacity of solid phase C_n , the volumetric heat capacity of organic matter C_o , the

711

volumetric heat capacity of liquid phase C_w , and empirical parameters b_1 , b_2 , and b_3) for heat

712

transport simulation.

Depth (cm)	θ_n (cm ³ cm ⁻³)	θ_o (cm ³ cm ⁻³)	λ_L (cm)	λ_T (cm)	b_1 (W cm ⁻¹ °C ⁻¹)	b_2 (W cm ⁻¹ °C ⁻¹)	b_3 (W cm ⁻¹ °C ⁻¹)	C_n (W cm ⁻¹ °C ⁻¹)	C_o (W cm ⁻¹ °C ⁻¹)	C_w (W cm ⁻¹ °C ⁻¹)
0-20	0.66	0	5	1	5.805E+11	2.113E+16	8.975E+16	1.43E+14	1.87E+14	3.12E+14
20-70	0.64	0	5	1	1.385E+16	2.494E+16	9.808E+16	1.43E+14	1.87E+14	3.12E+14

713

714

715

716

717

718

719

720

721

722

723

724

725

726

727

728

729

730

731

732

733

734

735

736

737

738

739

740

741

742

743

744

745

Table 4

746

The root mean square errors (RMSE), mean absolute errors (MAE), and mean relative errors

747

(MRE) between simulated and observed daily soil water contents for the P1, P2, and P3 treatments

748

at different positions by simulation with parameters estimated with soil textural information (S1),

749

soil water retention curve (S2), and Inverse model (S3).

Depth (cm)	Error	Treatment								
		P1			P2			P3		
		Top	Side	Base	Top	Side	Base	Top	Side	Base
S1										
0-10	RMSE (cm ³ cm ⁻³)	0.072	0.034	0.043	0.028	0.024	0.030	0.074	0.048	0.037
	MAE (cm ³ cm ⁻³)	0.064	0.025	0.038	0.022	0.019	0.023	0.064	0.042	0.031
	MRE (%)	51.8	15.3	25.3	11.8	9.4	9.2	51.1	25.1	15.7
10-20	RMSE (cm ³ cm ⁻³)	0.031	0.028	0.055	0.034	0.028	0.039	0.037	0.020	0.024
	MAE (cm ³ cm ⁻³)	0.026	0.024	0.052	0.028	0.019	0.033	0.030	0.017	0.021
	MRE (%)	12.6	14.0	36.7	13.0	8.0	19.9	17.1	7.1	11.1
20-30	RMSE (cm ³ cm ⁻³)	0.037	0.052	0.058	0.038	0.028	0.022	0.019	0.017	0.016
	MAE (cm ³ cm ⁻³)	0.033	0.049	0.055	0.034	0.024	0.017	0.017	0.014	0.015
	MRE (%)	19.3	33.7	40.3	13.3	10.2	7.2	6.9	7.2	7.3
30-50	RMSE (cm ³ cm ⁻³)	0.041	0.052	0.021	0.016	0.023	0.018	0.025	0.035	0.077
	MAE (cm ³ cm ⁻³)	0.038	0.050	0.019	0.014	0.020	0.018	0.025	0.035	0.077
	MRE (%)	24.5	34.7	8.9	7.1	11.3	8.0	12.9	19.0	26.0
S2										
0-10	RMSE (cm ³ cm ⁻³)	0.110	0.072	0.081	0.065	0.061	0.038	0.117	0.095	0.066
	MAE (cm ³ cm ⁻³)	0.100	0.063	0.072	0.060	0.055	0.032	0.107	0.091	0.052
	MRE (%)	78.5	35.7	47.1	31.3	27.7	14.5	82.0	52.1	28.5
10-20	RMSE (cm ³ cm ⁻³)	0.058	0.072	0.073	0.059	0.048	0.068	0.086	0.051	0.069
	MAE (cm ³ cm ⁻³)	0.048	0.065	0.065	0.050	0.044	0.058	0.079	0.045	0.063
	MRE (%)	24.7	37.4	45.5	25.0	20.7	35.1	42.7	20.3	32.9
20-30	RMSE (cm ³ cm ⁻³)	0.072	0.072	0.061	0.028	0.025	0.021	0.047	0.065	0.054
	MAE (cm ³ cm ⁻³)	0.063	0.063	0.056	0.024	0.021	0.017	0.042	0.059	0.049
	MRE (%)	37.5	43.2	40.9	10.1	9.2	7.5	18.7	29.8	24.7
30-50	RMSE (cm ³ cm ⁻³)	0.017	0.035	0.009	0.019	0.021	0.018	0.061	0.068	0.047
	MAE (cm ³ cm ⁻³)	0.013	0.034	0.008	0.014	0.017	0.017	0.055	0.065	0.044
	MRE (%)	8.5	23.2	3.6	7.5	9.2	7.6	29.1	36.1	14.8
S3										
0-10	RMSE (cm ³ cm ⁻³)	0.033	0.039	0.044	0.038	0.049	0.031	0.033	0.025	0.038
	MAE (cm ³ cm ⁻³)	0.026	0.034	0.040	0.034	0.045	0.023	0.027	0.020	0.032
	MRE (%)	21.6	15.8	26.2	16.2	20.1	9.5	20.8	9.7	16.1
10-20	RMSE (cm ³ cm ⁻³)	0.052	0.031	0.057	0.034	0.025	0.039	0.030	0.020	0.022
	MAE (cm ³ cm ⁻³)	0.046	0.028	0.055	0.027	0.017	0.032	0.024	0.017	0.020
	MRE (%)	19.3	16.1	38.5	11.2	6.9	19.7	11.5	6.9	10.4
20-30	RMSE (cm ³ cm ⁻³)	0.041	0.056	0.061	0.031	0.025	0.022	0.019	0.016	0.015
	MAE (cm ³ cm ⁻³)	0.037	0.054	0.058	0.028	0.022	0.016	0.016	0.014	0.014
	MRE (%)	21.9	36.8	42.4	10.9	9.2	7.0	6.9	6.9	7.0
30-50	RMSE (cm ³ cm ⁻³)	0.046	0.056	0.021	0.017	0.025	0.017	0.027	0.035	0.078
	MAE (cm ³ cm ⁻³)	0.043	0.053	0.018	0.015	0.022	0.017	0.026	0.035	0.077
	MRE (%)	27.5	37.2	8.7	8.1	12.1	7.4	13.5	19.1	26.1

750 **Table 5**
751 The root mean square errors (RMSE), mean absolute errors (MAE), and mean relative errors
752 (MRE) between simulated and observed daily soil temperatures for the P1, P2, and P3 treatments
753 at different positions.

Depth (cm)	Error	Treatment					
		P1		P2		P3	
		Top	Side	Top	Side	Top	Side
5	RMSE (°C)	2.7	4.2	3.9	3.3	2.0	4.2
	MAE (°C)	2.6	4.1	3.5	3.1	1.7	4.0
	MRE (%)	13.6	22.7	18.9	21.0	9.2	21.5
10	RMSE (°C)	1.1	2.5	2.5	2.1	1.2	1.5
	MAE (°C)	0.9	2.4	1.9	1.5	0.8	1.0
	MRE (%)	5.2	13.0	10.6	9.4	4.5	5.6
20	RMSE (°C)	1.2	1.1	4.0	2.1	1.5	1.6
	MAE (°C)	1.0	1.0	2.9	1.6	1.3	1.4
	MRE (%)	5.3	5.5	25.5	9.1	7.2	8.0
30	RMSE (°C)	1.2	1.3	1.7	1.5	1.9	1.5
	MAE (°C)	0.9	1.1	1.3	1.2	1.7	1.3
	MRE (%)	4.3	6.5	7.2	6.6	10.1	7.6
50	RMSE (°C)	1.4	1.0	1.9	1.1	2.2	2.2
	MAE (°C)	1.2	0.8	1.6	0.9	2.0	2.1
	MRE (%)	7.6	4.4	9.2	5.5	12.6	12.7

754

755